On-off switch and sign change for a nonlocal Josephson diode in spin-valve Andreev molecules

Erik Wegner Hodt * and Jacob Linder
Department of Physics, Center for Quantum Spintronics, Norwegian University of Science and Technology, NO-7491 Trondheim, Norway

(Received 30 June 2023; revised 2 October 2023; accepted 17 October 2023; published 1 November 2023)

Andreev molecules consist of two coherently coupled Josephson junctions and permit nonlocal control over supercurrents. By making the barriers magnetic and thus creating a spin valve, we predict that a nonlocal Josephson diode effect occurs that is switchable via the magnetic configuration of the barriers. The diode effect is turned on, off, or changes its sign depending on whether the spin valve is in a parallel, normal, or antiparallel configuration. These results offer a way to exert complete control over a nonlocal Josephson diode effect via the spin degree of freedom.

DOI: 10.1103/PhysRevB.108.174502

I. INTRODUCTION

The flow of a supercurrent between superconductors separated by a nonsuperconducting restriction—the Josephson effect [1]—is a striking depiction of the quantum nature of the superconducting state, and its physical implementation—the Josephson junction—is a fundamental device in quantum technology applications such as magnetic field sensing and metrology [2–4].

The interaction between multiple Josephson junctions (JJs) located within a distance on the order of the superconducting coherence length ξ_0 is an emerging field of interest. While there are numerous works on diverse nonlocal effects in systems with several Josephson junctions, several works have considered a particular model system known as the Andreev molecule, both theoretically [5–11] and experimentally [12–18]. The Andreev molecule is formed by the hybridization of overlapping Andreev bound states (ABSs) stemming from individual JJs separated by a distance on the order of ξ_0. The Andreev molecule has been predicted to depict a nonlocal Josephson effect due to the nonlocal interaction between the phase gradients over the two JJs [5], causing a deviation from the single-junction current-phase relation and a nonreciprocal critical current. This can be viewed as a nonlocally induced superconducting diode effect.

The superconducting diode effect, the observation of an asymmetry between the forward and reverse critical currents $I_{c+} \neq I_{c-}$, is believed to be an important building block in future, dissipationless electronics devices. The effect was observed for a bulk system by Ando *et al.* [19] and was attributed to a magnetochiral anisotropy, caused by the breaking of time and spatial inversion symmetries. Apart from properties of bulk superconductors, there have been several predictions of rectifying behavior in Josephson junction based systems; for instance, Refs. [20–28] where the sources of the asymmetry are diverse, originating in magnetic barriers, sample geometry, and the presence of spin-orbit coupling among others. As indicated by Pillet *et al.* [5], the nonlocal modulation of the current-phase relation in an Andreev molecule also introduces an asymmetry between the positive and negative critical currents. As such, the Andreev molecule is an interesting system for the study and realization of the superconducting diode effect. However, the role of the spin degree of freedom has not been addressed so far in the literature on this system.

In this paper, we introduce the spin-valve Andreev molecule, consisting of three superconducting regions separated by spin-active barriers [see Fig. 1(a)]. The relative orientation of the magnetic moment on the two barriers can be rotated in experimental setups and we show that the rectifying behavior of the spin-valve Andreev molecule changes significantly when the magnetic barriers are parallel (P), normal to each other (N), or antiparallel (AP). We show that by switching the relative magnetization from P to (1) N and (2) AP, the diode effect in the molecule can be (1) switched off and (2) reversed, with comparable diode efficiency in the other direction. This shows that the spin degree of freedom in coherently coupled Josephson junctions can be used to obtain new functionality, offering full control over the diode effect.

II. MODEL

The spin-valve Andreev molecule consists of three one-dimensional (1D) superconductors connected by ferromagnetic weak links, as depicted in Fig. 1(a). The phase differences between the superconducting order parameters across each weak link are fixed for the middle superconductor by a connection to ground. If the weak links are separated by a distance on the order of the superconducting coherence length ξ_0, the phase difference across one weak link can affect the "effective" phase over the other through hybridization of the ABSs centered at each weak link. The spin-active barriers serving as the weak links are modeled as Dirac δ functions.

We model the SFSFS spin-valve Andreev molecule using the Bogoliubov–de Gennes formalism [29]. Due to the spin

*Corresponding author: erik.w.hodt@ntnu.no

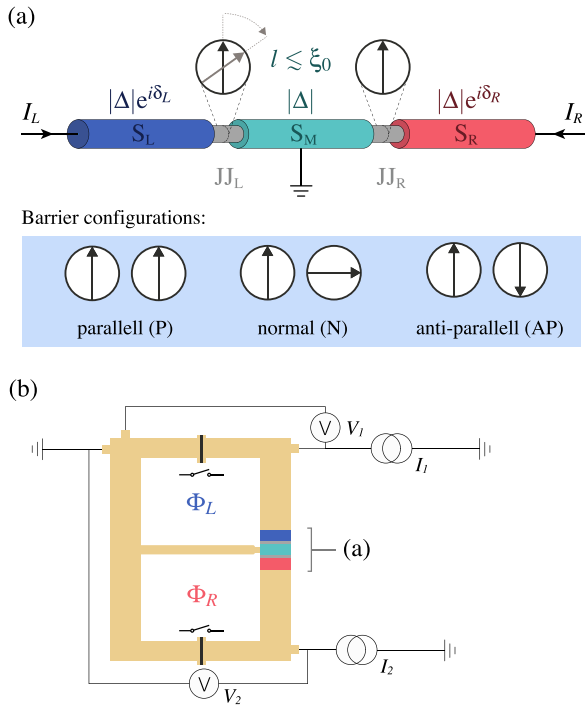

FIG. 1. (a) The spin-valve Andreev molecule consists of three 1D superconductors where the phase difference between the superconducting order parameters is fixed. By a relative rotation of the magnetic moments of the spin-active barriers separating the three superconducting regions, drastically different superconducting diode characteristics can be achieved in the molecule. (b) Experiment proposal for characterizing the spin-valve Andreev molecule. By pinching off the uppermost current loop, the phase difference between the middle and right superconductors can be fixed with a magnetic flux Φ_R.

splitting induced by the ferromagnetic barriers, we consider the full 4×4 Nambu space Hamiltonian

$$H = \begin{pmatrix} H_0 + V_{\uparrow\uparrow} & V_{\uparrow\downarrow} & 0 & \Delta \\ V_{\downarrow\uparrow} & H_0 + V_{\downarrow\downarrow} & -\Delta & 0 \\ 0 & -\Delta^* & -H_0 - V_{\uparrow\uparrow} & -V^*_{\uparrow\downarrow} \\ \Delta^* & 0 & -V^*_{\downarrow\uparrow} & -H_0 - V_{\downarrow\downarrow} \end{pmatrix}, \tag{1}$$

where the gap parameter $\Delta(x)$ and potentials $V_{\alpha\beta}(x)$ are defined by

$$\Delta(x) = \begin{cases} |\Delta| e^{i\delta_L} & \text{if } x < -l/2 \\ 0 & \text{if } |x| < l/2 \\ |\Delta| e^{i\delta_R} & \text{if } x > l/2, \end{cases} \tag{2}$$

$$V_{\alpha\beta} = U_L(\sigma_0 + \gamma \hat{n}_L \cdot \boldsymbol{\sigma})_{\alpha\beta}\delta(x + l/2) + U_R(\sigma_0 + \gamma \hat{n}_R \cdot \boldsymbol{\sigma})_{\alpha\beta}\delta(x - l/2), \tag{3}$$

where $H_0 = \frac{-\hbar^2}{2m}\partial_x^2 - \mu$, l is the length of the middle superconductor, U_0 is the spin-independent barrier potential, and $0.0 < \gamma < 1.0$ denotes the strength of the spin-active potential relative to U_L/U_R. Moreover, m is the electron mass, μ the chemical potential, $\hat{n}_{L/R}$ the unit vector denoting the direction of the left/right barrier moment, and $\boldsymbol{\sigma}$ the vector of Pauli matrices while σ_0 is the identity matrix. We will only consider situations where the spin-independent barriers are symmetric, $U_L = U_R = U_0 = 0.25\hbar v_F$ where v_F is the Fermi velocity. For the nonmagnetic Andreev molecule, this barrier strength corresponds to a transmission probability of $\tau = 0.94$, which is considered realistic for single-channel conductors such as InAs-Al nanowires [30].

It could also be interesting to include the role of spin-orbit interactions in the superconducting regions in future studies. However, as has been noted in previous literature [31], experiments have reported [32] a spin-orbit energy in, e.g., InAs nanowires, which is, at most, of order 100 μeV. In contrast, the proximity-induced superconducting gap in In-based nanowires has been reported [33] to be as high as 500 μeV. Therefore, a model where the spin-orbit interactions are neglected relative to the superconducting gap is warranted, since such a scenario should be experimentally feasible based on previous reports in the literature. Regarding the experimental aspect of controllable spin barriers, this has been demonstrated earlier in the literature [34] in the context of spin-valve Josephson junction. So long as the barriers differ in some respect, either geometrically (shape or thickness) or in terms of material choice, their magnetic switching fields will be different, thus allowing control of the relative magnetic configuration.

The diode efficiency is quantified by the difference in critical supercurrent in the positive and negative directions, $\Delta I_c = I_{c+} - I_{c-}$ and the diode efficiency is commonly defined as [35]

$$\eta \equiv \frac{\Delta I_c}{I_{c+} + I_{c-}}. \tag{4}$$

Solving Eq. (1) in each of the three superconductors and using appropriate boundary conditions at the interfaces (see the Appendices for details), one obtains the discrete subgap ($E < |\Delta|$) energy levels known as Andreev bound states as well as a continuum of states for energies $E > |\Delta|$. We make the common semiclassical approximation $\xi_0 \gg \lambda_F$ where λ_F is the Fermi wavelength and choose the Fermi momentum such that $k_F l = \pi/2 \bmod 2\pi$, $k_F l \gg 1$. The two barriers of the Andreev molecule form an effective Fabry-Perot resonator and the transmission τ is affected by whether $k_F l = 0 \,(\text{mod } 2\pi)$ (on resonance) or $k_F l = \pi/2 \,(\text{mod } 2\pi)$ (off resonance) [5,8]. The results below are obtained in the off-resonance condition (resonance is discussed in the Appendices). For the spin-valve Andreev molecule, the coupling of the independent plane-wave solutions in each superconductor involves solving for 16 coefficients giving the weight of the electron- and hole-type plane waves of spin up/spin down. The results shown in this paper are calculated numerically.

III. RESULTS AND DISCUSSION

As the length of the middle superconductor in the Andreev molecule becomes on the order of the superconducting coherence length ξ_0, the ABSs located at each of the two Josephson junctions hybridize. The ABS for the regular Andreev molecule without magnetic barriers is shown in Fig. 2 for middle superconductor lengths $l \gg \xi_0$ and $l = \xi_0$. For long separations ($l \gg \xi_0$), the molecule behaves as two independent junctions with a regular, short weak-link $I_c \propto \sin(\delta_L)$

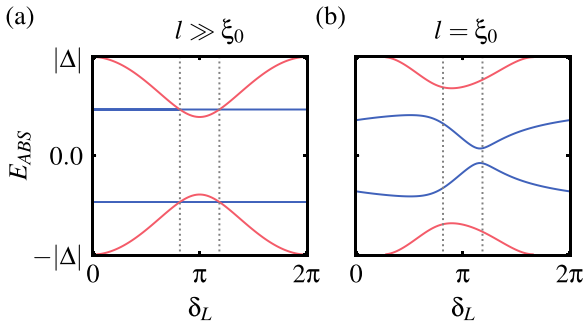

FIG. 2. Andreev bound states (ABSs) for the Andreev molecule with the length of the middle superconductor (a) significantly longer than, or (b) comparable to the superconducting coherence length ξ_0. For $l \gg \xi_0$, $E_{ABS}(\delta_L, \delta_R) \to E_{ABS}(\delta_L)$ for the ABSs localized at the left weak link as the nonlocal impact of δ_R diminishes. As l becomes on the order of ξ_0, the ABSs from the two junctions hybridize into Andreev molecule orbitals. These states feature avoided crossings at $\delta_L = \pm\delta_R$ (dotted lines) related to the emergence of double-crossed Andreev reflection (dCAR) and double elastic cotunneling (dEC) processes.

current-phase relation for the left junction while the ABS from the separated, right junction remain dispersionless under the variation of the local phase δ_L. This reflects the absence of nonlocal modulation for this setup. As l becomes on the order of a coherence length ($l = \xi_0$), the bands hybridize and avoided crossings arise at the previous band degeneracies at $\delta_L = \pm\delta_R$. These are caused by two distinct processes in the Andreev molecule: double-crossed Andreev reflection (dCAR) and double elastic cotunneling (dEC). dEC facilitates transmission of Cooper pairs through the molecule and occurs for $\delta_L = -\delta_R$ (i.e., the same phase gradient over both junctions) [36], while dCAR involves the creation of a Cooper pair in the middle superconductor by an incident electron from the left in the left superconductor and an Andreev reflected hole in the right superconductor for $\delta_L = \delta_R$, made possible by the length of the middle superconductor being on the order of the extent of the Cooper pair itself [8,37].

The magnetic barriers of the spin-valve Andreev molecule lift the spin degeneracy of the spin-up and spin-down states and have a significant effect on the ABS spectrum. The left junction current I_L, as well as the ABS, is shown in Fig. 3 for the parallel (P), normal (N), and antiparallel (AP) configurations, as depicted in Fig. 1. The nonlocal phase is fixed at $\delta_R = 2.56$, the value which gives the largest superconducting diode effect in the nonmagnetic Andreev molecule. As the barriers become spin active, the ABSs in the P configuration are spin split in a manner reminiscent of regular Zeeman-type splitting where the band curvature remains largely unchanged, except close to the gap $-\Delta$. This is significant because the current contribution from the ABS spectrum is proportional to the phase gradient of the ABS bands. The AP configuration experiences a similar splitting away from the avoided crossings at $\delta_L = \pm\delta_R$, but due to a retained spin degeneracy at those points, the phase gradient of the ABS is more affected in this case. An additional important consequence of the magnetic barriers is that for the P configuration, the gap at the Fermi level ($E_{ABS} = 0.0$) closes for a critical barrier strength $\gamma \simeq 0.3$. As a consequence, the ABS spectrum for the P configuration displays band inversion above this threshold, causing a cancellation of the current contribution due to the two upper bands in the ABS spectrum. For a regular Josephson junction, ABS spin splitting has no rectifying effect on the current-phase relation due to a symmetry around $\delta_L = \pi$. In the Andreev molecule, this symmetry is broken due to the nonlocal modulation from δ_R, causing the band inversion to

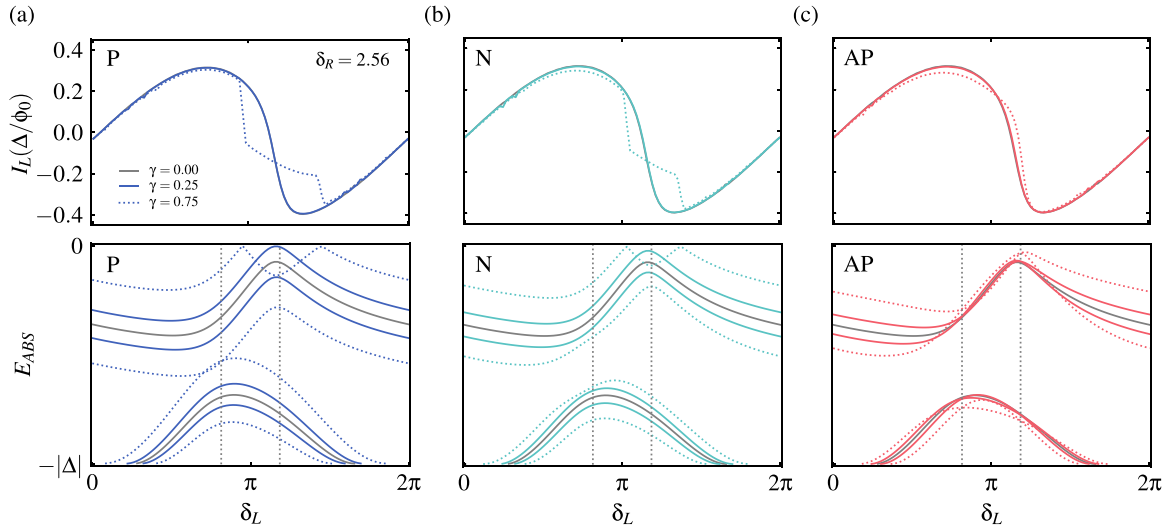

FIG. 3. Current through the left junction as well as the subgap Andreev bound states (ABSs) as a function of local phase δ_L for barrier strengths $\gamma = 0.00$, $\gamma = 0.25$, and $\gamma = 0.75$ for the parallel (a), normal (b), and antiparallel (c) configurations. The nonlocal phase is set at $\delta_R = 2.56$. As the strength of the magnetic barrier increases, the P ABS experiences a Zeeman-like spin splitting, leading to current discontinuities caused by band inversion as the gap between the ABS at the Fermi level closes at a critical value $\gamma \simeq 0.3$. In contrast, the AP configuration retains its spin degeneracy at the points $\delta_L = \pm\delta_R$ (black dotted lines) and the Fermi level gap remains open for all parameters investigated but with a reduced I_{c+} due to spin-splitting induced mismatch in the phase gradient of the four bands. The N configuration ABS depicts both the reduction in I_{c+} from AP and the band inversion and current discontinuities from N, behaving as an effective mix of the two extrema.

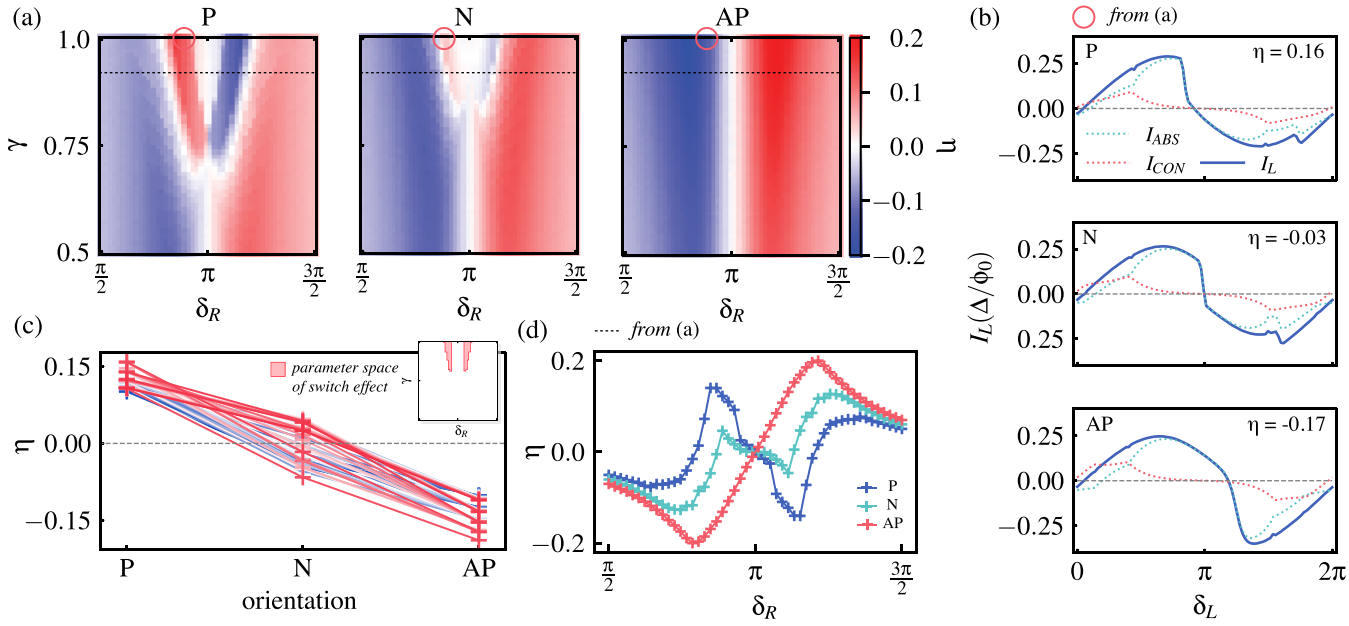

FIG. 4. On-off switch as well as sign change in the nonlocal Josephson diode efficiency is shown for a spin-valve Andreev molecule with $l = \xi_0$. (a) The diode efficiency dependence on the nonlocal phase δ_R and spin splitting of the barrier γ shows that significant deviations arise between the three configurations for $\gamma > 0.5$. (b) The JJ_L current-phase relation is shown for the parameter region denoted by red rings in (a). For specific combinations of δ_R and γ shown in (c), $\eta > 0.1$ for the P configuration, $-0.1 < \eta < 0.1$ for N, and $\eta < -0.1$ for the AP configuration. This enables an effective on-off switching as well as sign change of the diode efficiency by an appropriate rotation of the spin-valve configuration. (d) The diode efficiency is shown as a function of nonlocal phase δ_R along the dotted line in (a), for $\gamma \simeq 0.9$, highlighting the asymmetry between the three configurations.

have an impact also on the rectifying behavior of the nonlocal Josephson effect.

We now demonstrate that the combination of the magnetic barriers and the nonlocal current-phase modulation in the spin-valve Andreev molecule constitutes a novel route for exerting complete control of the superconducting diode effect: both its existence and its sign can be tuned *in situ* via the spin-valve configuration. The diode efficiency in the critical current through the left junction is shown as a function of the nonlocal phase δ_R in Fig. 4 for a system with length $l = \xi_0$ (the diode efficiency dependence on the middle superconductor length l is shown in the Appendices). For values of the spin-active barrier strength $\gamma < 0.5$ (see additional data in the Appendices), the three barrier configurations show similar diode efficiency characteristics, but a significant asymmetry in the diode behavior arises above $\gamma = 0.5$. While the diode efficiency of the AP configuration increases monotonously with γ, the diode efficiency of the P configuration depicts a reversion phenomenon for δ_R close to π, as is evident from Fig. 4(a). The combined effect of the breaking of symmetry in the current-phase relation around $\delta_L = \pi$ as well as the barrier-induced band inversion and subsequent partial cancellation of the ABS phase gradients for $\delta_L > \pi$ cause the negative critical current I_{c-} to reduce in magnitude for the P configuration. This makes the originally negative diode efficiency zero and then positive for $\gamma > 0.5$ in the interval $\frac{3\pi}{4} < \delta_R < \pi$. The behavior for $\delta_R > \pi$ is equivalent but with the opposite sign. For the N configuration, the combination of a weaker band inversion effect as well as a reduction in critical positive current I_{c+} [see Fig. 3(b), upper panel] effectively establishes a region of vanishing diode efficiency. The junction current in this parameter region is shown for the P, N, and AP configuration in Fig. 4(b).

As a metric of the extent of this effect, we show the region of δ_R and γ for which an on-off effect as well as switching with a P/AP threshold efficiency of $\eta_{\text{lim}} > |0.1|$ and N efficiency of $-0.1 < \eta_{\text{lim}} < 0.1$ is achievable. Figure 4(c) shows the diode efficiency for these specific δ_R and γ and their respective efficiency in the parallel, normal, and antiparallel configurations. The inset shows where in the diagrams in Fig. 4(a) both the on-off and the switching effects are observed. We note that this parameter region increases significantly if the threshold efficiency η_{lim} is lowered or if one relinquishes the need for a vanishing normal diode efficiency and only considers the switching between positive and negative diode efficiency for the P and AP configurations.

To conclude, we propose an on-off and switching mechanism in the superconducting diode effect of a spin-valve Andreev molecule. This occurs due to the interplay between nonlocal phase modulation from the regular Andreev molecule and the introduction of magnetic barriers which alters the ABS spectrum of the molecule. The combination of a vanishing Fermi level gap and subsequent band inversion with nonlocal phase modulation in the parallel configuration Andreev molecule causes a reversion of the diode efficiency which establishes a parameter region where the magnitude and sign of the diode efficiency can be tuned by relative rotation of the magnetic barrier moments. This entails the possibility of a device where one can switch on-off as well as reverse the diode efficiency for a constant phase-bias δ_R.

ACKNOWLEDGMENTS

We thank C. Brüne and N. Birge for helpful comments. This work was supported by the Research Council of Norway through Grant No. 323766 and its Centres of Excellence funding scheme Grant No. 262633 QuSpin. Support from Sigma2, the National Infrastructure for High Performance Computing and Data Storage in Norway, Project No. NN9577K, is acknowledged. The research presented in this paper has benefited from the Experimental Infrastructure for Exploration of Exascale Computing (eX3), which is financially supported by the Research Council of Norway under Contract No. 270053.

APPENDIX A: CALCULATION OF ANDREEV BOUND STATE CURRENT

The wave functions in each of the three superconductors are constructed with spin-full electron/hole plane waves, which are eigenstates of an infinite superconductor. For positive energies, the plane waves are given by

$$\begin{aligned}
\psi^{\delta\pm}_{e,\uparrow}(x) &= \frac{1}{\sqrt{L}}(u_0 e^{-i\delta/2}, 0, 0, v_0 e^{i\delta/2})^T e^{\pm ik^+x},\\
\psi^{\delta\pm}_{h\downarrow}(x) &= \frac{1}{\sqrt{L}}(v_0 e^{-i\delta/2}, 0, 0, u_0 e^{i\delta/2}) e^{\mp ik^-x},\\
\psi^{\delta\pm}_{e,\downarrow}(x) &= \frac{1}{\sqrt{L}}(0, u_0 e^{-i\delta/2}, -v_0 e^{i\delta/2}, 0) e^{\pm ik^+x},\\
\psi^{\delta\pm}_{h\uparrow}(x) &= \frac{1}{\sqrt{L}}(0, -v_0 e^{-i\delta/2}, u_0 e^{i\delta/2}, 0) e^{\mp ik^-x},
\end{aligned} \tag{A1}$$

where the coherence factors u_0, v_0 are defined as

$$u_0 = \frac{1}{\sqrt{2}}\left(1 + \frac{\sqrt{E^2-\Delta^2}}{E}\right)^{1/2}, \tag{A2}$$

$$v_0 = \frac{1}{\sqrt{2}}\left(1 - \frac{\sqrt{E^2-\Delta^2}}{E}\right)^{1/2}, \tag{A3}$$

where E is the Bogoliubov–de Gennes energy eigenvalue. For negative energies, the wave functions are modified and become

$$\begin{aligned}
\psi^{\delta\pm}_{e,\uparrow}(x) &= \frac{1}{\sqrt{L}}(-v_0^* e^{-i\delta/2}, 0, 0, u_0^* e^{i\delta/2}) e^{\mp ik^-x},\\
\psi^{\delta\pm}_{h\downarrow}(x) &= \frac{1}{\sqrt{L}}(-u_0^* e^{-i\delta/2}, 0, 0, v_0^* e^{i\delta/2}) e^{\pm ik^+x},\\
\psi^{\delta\pm}_{e,\downarrow}(x) &= \frac{1}{\sqrt{L}}(0, -v_0^* e^{-i\delta/2}, -u_0^* e^{i\delta/2}, 0) e^{\mp ik^-x}.\\
\psi^{\delta\pm}_{h\uparrow}(x) &= \frac{1}{\sqrt{L}}(0, u_0^* e^{-i\delta/2}, v_0^* e^{i\delta/2}, 0) e^{\pm ik^+x}.
\end{aligned} \tag{A4}$$

We assume that $\xi_0 \gg \lambda_F$ where ξ_0 is the superconducting coherence length and λ_F is the Fermi wavelength. We may approximate the wave vector of the electron and hole plane waves k^+, k^- as $k^+ \simeq k_f + i\sqrt{1-\epsilon^2}/\xi_0$, $k^- \simeq k_f - i\sqrt{1-\epsilon^2}/\xi_0$ where the coherence length is defined as $\xi_0 = \hbar v_F/\Delta$. Note that for subgap states, $-1 < \epsilon < 1$ where $\epsilon = E/|\Delta|$, causing the wave vector to become complex. The complex nature of the subgap wave vector reflects that the ABS is confined to the vicinity of the junction, vanishing in the superconductor bulk.

The wave function in the spin-valve Andreev molecule is now given by

$$\psi(x) = \begin{cases}
c_1\psi^{\delta_l-}_{e,\uparrow} + c_2\psi^{\delta_l-}_{e,\downarrow} + c_3\psi^{\delta_l+}_{h,\uparrow} + c_4\psi^{\delta_l+}_{h,\downarrow} & x < -l/2\\
c_5\psi^{0-}_{e,\uparrow} + c_6\psi^{0-}_{e,\downarrow} + c_7\psi^{0+}_{h,\uparrow} + c_8\psi^{0+}_{h,\downarrow} & \\
c_9\psi^{0+}_{e,\uparrow} + c_{10}\psi^{0+}_{e,\downarrow} + c_{11}\psi^{0-}_{h,\uparrow} + c_{12}\psi^{0-}_{h,\downarrow} & |x| < l/2\\
c_1\psi^{\delta_l-}_{e,\uparrow} + c_2\psi^{\delta_l-}_{e,\downarrow} + c_3\psi^{\delta_l+}_{h,\uparrow} + c_4\psi^{\delta_l+}_{h,\downarrow} & x < -l/2,
\end{cases} \tag{A5}$$

where diverging solutions for $x \to \pm\infty$ are excluded. The total wave function must be continuous at the boundaries

$$\psi(\pm l/2^+) = \psi(\pm l/2^-) \tag{A6}$$

and the wave function derivatives must, due to the Dirac delta barriers, satisfy the following relation:

$$\partial_x\psi(\pm l/2^+) - \partial_x\psi(\pm l/2^-) = \frac{2m}{\hbar}U_{R/L}\psi(\pm l/2). \tag{A7}$$

Upon matching the wave function $\psi(x)$ at the two boundaries in the spin-valve Andreev molecule, a homogeneous equation set of 16 equations is obtained which can be solved for the 16 coefficients $c_1 \ldots c_{16}$. This was done numerically in this project by requiring the determinant of the coefficient matrix to be zero in order for a nontrivial solution.

From the approach above, one obtains up to eight distinct energies ϵ, and the contribution to the Josephson current from the ABS spectrum is given by the phase gradient of the free energy [38]

$$I(\delta_L, \delta_R) = -\frac{e}{\hbar}\sum_{\epsilon<0}\frac{\partial\epsilon(\delta_L,\delta_R)}{\partial\delta_L}\tanh\left(\frac{\epsilon}{2k_BT}\right), \tag{A8}$$

where the ABS energies depend on both the local and the nonlocal phases δ_L, δ_R due to the Andreev molecule hybridization. The current contribution comes from occupied states, which for $T = 0$ is $\epsilon < 0$. It then follows that $\tanh(\frac{\epsilon}{2k_BT}) \to -1$, so that the ABS contribution can be written more simply as

$$I(\delta_L, \delta_R) = \frac{e}{\hbar}\sum_{\epsilon<0}\frac{\partial\epsilon(\delta_L,\delta_R)}{\partial\delta_L}. \tag{A9}$$

APPENDIX B: CALCULATION OF CONTINUUM CURRENT

For the calculation of the continuum current, we use the same electron and hole plane waves given by Eqs. (A1)–(A4), but as we now consider states in the continuum, the plane waves are not evanescent. The electron and hole wave vectors may be approximated as $k^+ \simeq k_f + \sqrt{\epsilon^2-1}/\xi_0$, $k^- \simeq k_f - \sqrt{\epsilon^2-1}/\xi_0$ with the coherence length defined as $\xi_0 = \hbar v_F/\Delta$. We are in effect considering a scattering problem with incoming waves $\psi_{\rm inc}(x)$ which are scattered to outgoing waves $\psi_{\rm out}(x)$ at the barriers,

$$\psi(x) = \psi_{\rm inc}(x) + \psi_{\rm out}(x). \tag{B1}$$

The outgoing waves are identical with the wave function constructed for the ABS in Eq. (5) (except for the wave vectors k_e/k_h now being real), but we must now also consider eight

distinct types of incoming waves,

$$\psi^{e}_{\text{inc}}(x) = \begin{cases} \psi^{\delta_L +}_{e,\uparrow/\downarrow} & \text{if } x < -l/2 \\ \psi^{\delta_L -}_{h,\uparrow/\downarrow} & \text{if } x < -l/2 \\ \psi^{\delta_R -}_{e,\uparrow/\downarrow} & \text{if } x > l/2 \\ \psi^{\delta_R +}_{h,\uparrow/\downarrow} & \text{if } x > l/2. \end{cases} \tag{B2}$$

where each wave has a spin-up and spin-down version.

For each of the eight incoming waves in Eq. (B2), we construct the total wave function from Eq. (B1) and solve for the 16 coefficients $c_1 \dots c_{16}$. This yields the total wave function

$$\psi(x) = \frac{1}{\sqrt{L}} \begin{pmatrix} u_\uparrow(x) \\ u_\downarrow(x) \\ v_\uparrow(x) \\ v_\downarrow(x) \end{pmatrix} \tag{B3}$$

for the eight distinct cases. We may calculate the current contribution from the continuum states using the following general expression for the current:

$$\boldsymbol{j} = \frac{e}{2m} \sum_\sigma \langle \Psi^\dagger_\sigma \hat{\boldsymbol{p}} \Psi_\sigma + (\hat{\boldsymbol{p}}^\dagger \Psi^\dagger_\sigma) \Psi_\sigma \rangle. \tag{B4}$$

Using now that $\Psi_\sigma = \sum_k [u_{n\sigma}(x)\gamma_k - \sigma v^*_{k\sigma}(x)\gamma_k^\dagger]$ and that $\langle \gamma_k^\dagger \gamma_k \rangle = f(E_k)$, we obtain

$$\begin{aligned} \boldsymbol{j} = \frac{\hbar e}{m} \sum_{k,\sigma} & \text{Im}\big[u^*_{k\sigma}(x)\partial_x u_{k\sigma}(x)\big] f(E_k) \\ & + \text{Im}[v^*_{k\sigma}(x)\partial_x v_{k\sigma}(x)][1 - f(E_k)]. \end{aligned} \tag{B5}$$

Assuming now that $T = 0$, only the holelike components $v_{k\sigma}$ will contribute to the current. We let $\sum_k \to \int dk \frac{L}{2\pi}$ and turn to an integral over energy by using that $d\zeta/dk \simeq \hbar^2 k_f/m$ and $d\zeta/dE = \frac{E}{\sqrt{E^2-\Delta^2}} = \frac{\epsilon}{\sqrt{\epsilon-1}}$. The expression for the current contribution from the continuum becomes

$$I(x) = \frac{1}{2\phi_0} \sum_\sigma \int_1^\infty \frac{d\epsilon}{2\pi k_f} \frac{\epsilon}{\sqrt{\epsilon - 1}} \text{Im}[v^*_{\epsilon\sigma}(x)\partial_x v_{\epsilon\sigma}(x)], \tag{B6}$$

where $\phi_0 = \hbar/2e$. The current through the left junction can now be evaluated by taking $x = -l/2$ and evaluating Eq. (B6) for all incoming waves defined in Eq. (B2).

APPENDIX C: DIODE EFFECT DEPENDENCE ON k_F

The properties of the Andreev molecule are dependent on the value (mod 2π) chosen for the Fermi momentum k_F. In the main text, a value $k_F = \pi/2 \bmod 2\pi$, $k_F l \gg 1$ was found to give the most interesting results, corresponding to the off-resonance case discussed by Refs. [5,8]. In effect, the value of $\pi/2$ corresponds to the case where there is no resonance in the effective Fabry-Perot cavity formed by the two barriers in the Andreev molecule. This is associated with a reduced transmission probability τ. Oppositely, the $k_F = 0.0 \bmod 2\pi$ case is on resonance and is associated with an increase in transmission probability compared to the bare barriers [5]. The results in the main text are presented for a $l = \xi_0$ system and diode efficiency diagrams analogous to Fig. 4(a) in the main text are shown in Fig. 5 for Fermi momentum values $k_F = \theta \bmod 2\pi$, $k_F l \gg 1$, $\theta \in [0, \frac{\pi}{2}]$.

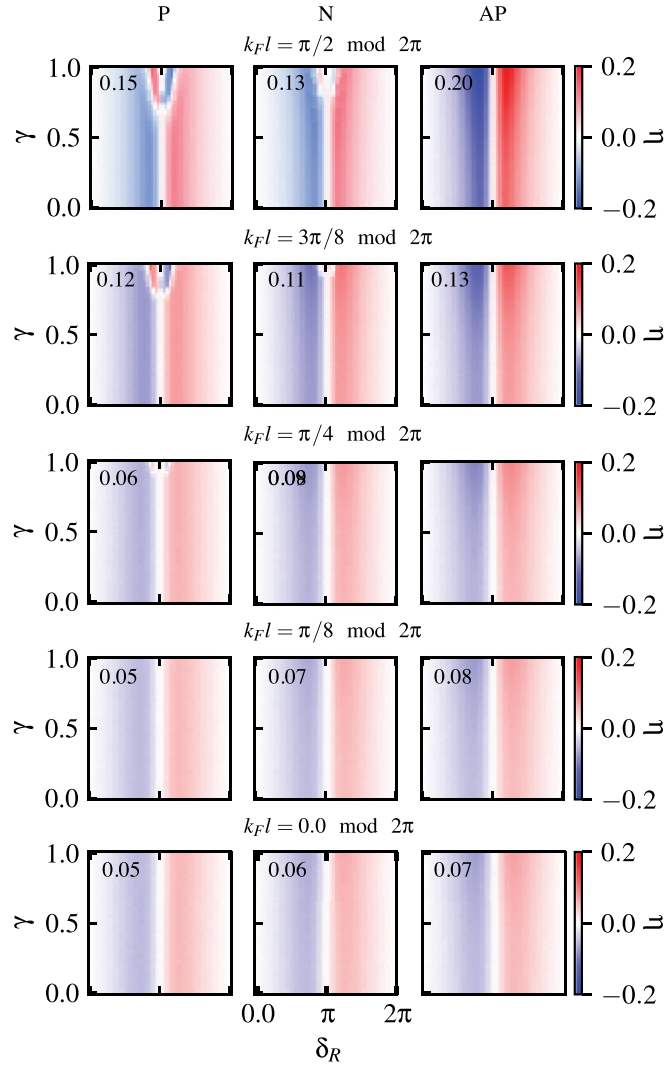

FIG. 5. Diode efficiencies for the parallel (P), normal (N), and antiparallel (AP) conditions for different choices of Fermi momentum, indicating the effect on the diode characteristics as the system deviates from the "off-resonance" condition $k_F = \pi/2 \bmod 2\pi$. The results indicate that the off-resonance condition is ideal for the switching effect due to the largest asymmetry between the P, N, and AP configurations. However, the effect can also persist when perturbed away from the $\pi/2$ condition.

From Fig. 5 it is clear that as θ moves away from the off-resonance condition, the asymmetries enabling the switching and sign-change effects become less significant and disappear for $\theta = \pi/4$. It is, however, also clear that the effect persists away from $\theta = \pi/2$ indicating that the observed effects are not a result of a "magic" parameter choice, but a more rigorous property of the system in the vicinity of the off-resonance condition.

APPENDIX D: DIODE EFFECT AS A FUNCTION OF l

The superconducting diode effect in the spin-valve Andreev molecule is dependent on the hybridization of the ABSs in the two junctions. It shows a strong dependence on the

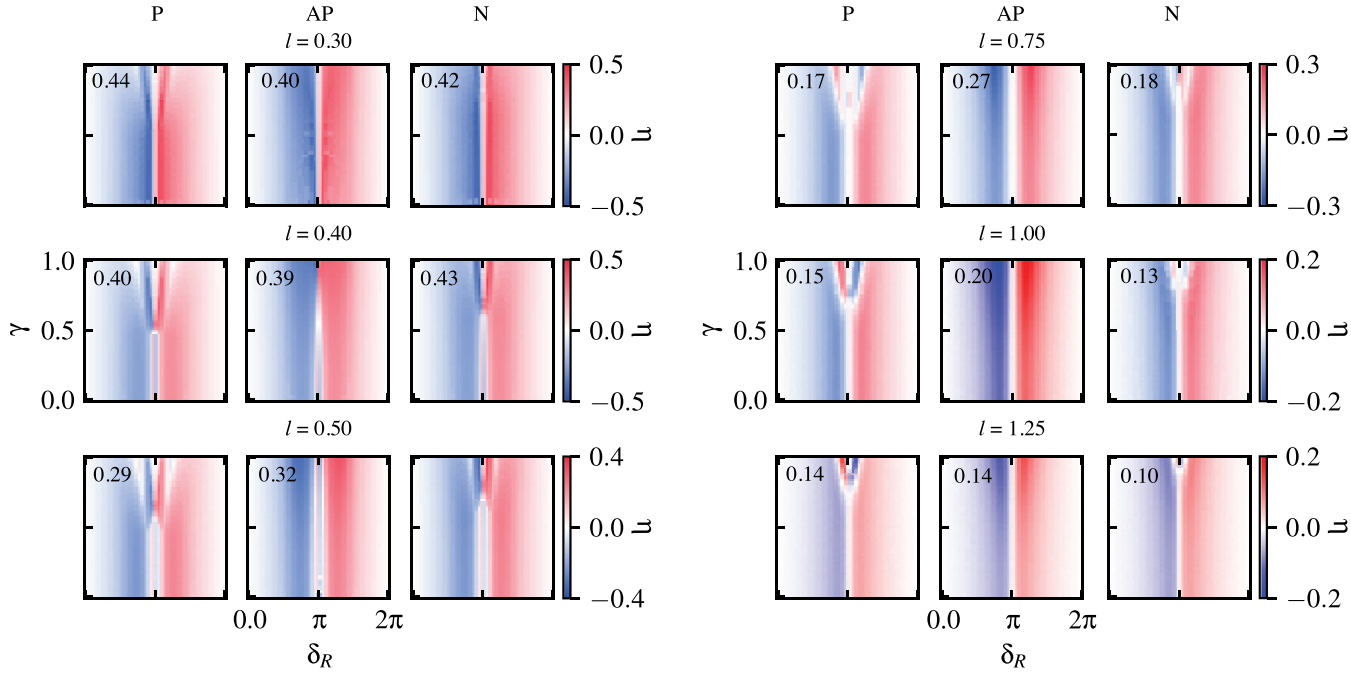

FIG. 6. Superconducting diode efficiency in the spin-valve Andreev molecule as a function of the middle superconductor length l. The maximum diode efficiency is denoted by the upper-left corner text. A significant increase in the diode efficiency is observed as l decreases, with a maximum diode efficiency of $\eta = 0.44$ observed for the parallel configuration at $l = 0.30\xi_0$.

middle superconductor length l. The diode efficiency is shown in Fig. 6 as a function of l ranging from 0.25 to $1.25\xi_0$. The diagram for $l = 1.00$ is a zoomed-out version of the data presented in the main text.

The results in Fig. 6 show that the largest observed diode efficiencies given symmetric barrier strengths of $U_0 = 0.25\hbar v_F$ is $\eta = 0.44$, observed for the $l = 0.30\xi_0$ N configuration. It is clear that while the diode characteristics change significantly with the middle superconductor length l, asymmetries in diode behavior between the different configurations persist, which can be utilized for selective control of the diode efficiency.

[1] K. K. Likharev, Rev. Mod. Phys. **51**, 101 (1979).
[2] G. Wendin, Rep. Prog. Phys. **80**, 106001 (2017).
[3] R. L. Fagaly, Rev. Sci. Instrum. **77**, 101101 (2006).
[4] B. Jeanneret and S. P. Benz, Eur. Phys. J.: Spec. Top. **172**, 181 (2009).
[5] J.-D. Pillet, V. Benzoni, J. Griesmar, J.-L. Smirr, and Ç. Ö. Girit, Nano Lett. **19**, 7138 (2019).
[6] A. Keliri and B. Douçot, Phys. Rev. B **107**, 094505 (2023).
[7] V. Kornich, H. S. Barakov, and Y. V. Nazarov, Phys. Rev. Res. **1**, 033004 (2019).
[8] J.-D. Pillet, V. Benzoni, J. Griesmar, J.-L. Smirr, and Ç. Ö. Girit, SciPost Phys. Core **2**, 009 (2020).
[9] E. Zsurka, N. Plaszkó, P. Rakyta, and A. Kormányos, 2D Mater. **10**, 035009 (2023).
[10] T. Chamoli and Ajay, Eur. Phys. J. B **95**, 163 (2022).
[11] J.-D. Pillet, S. Annabi, A. Peugeot, H. Riechert, E. Arrighi, J. Griesmar, and L. Bretheau, Phys. Rev. Res. **5**, 033199 (2023).
[12] S. Matsuo, J. S. Lee, C.-Y. Chang, Y. Sato, K. Ueda, C. J. Palmstrøm, and S. Tarucha, Commun. Phys. **5**, 221 (2022).
[13] S. Matsuo, T. Imoto, T. Yokoyama, Y. Sato, T. Lindemann, S. Gronin, G. C. Gardner, S. Nakosai, Y. Tanaka, M. J. Manfra, and S. Tarucha, arXiv:2303.10540.
[14] O. Kürtössy, Z. Scherübl, G. Fülöp, I. E. Lukács, T. Kanne, J. Nygård, P. Makk, and S. Csonka, Nano Lett. **21**, 7929 (2021).
[15] Z. Scherübl, A. Pályi, and S. Csonka, Beilstein J. Nanotechnol. **10**, 363 (2019).
[16] Z. Su, A. B. Tacla, M. Hocevar, D. Car, S. R. Plissard, E. P. A. M. Bakkers, A. J. Daley, D. Pekker, and S. M. Frolov, Nat. Commun. **8**, 585 (2017).
[17] S. Matsuo, T. Imoto, T. Yokoyama, Y. Sato, T. Lindemann, S. Gronin, G. C. Gardner, M. J. Manfra, and S. Tarucha, arXiv:2305.06596.
[18] S. Matsuo, T. Imoto, T. Yokoyama, Y. Sato, T. Lindemann, S. Gronin, G. C. Gardner, M. J. Manfra, and S. Tarucha, Nat. Phys. (2023), doi: 10.1038/s41567-023-02144-x.
[19] F. Ando, Y. Miyasaka, T. Li, J. Ishizuka, T. Arakawa, Y. Shiota, T. Moriyama, Y. Yanase, and T. Ono, Nature (London) **584**, 373 (2020).
[20] A. A. Reynoso, G. Usaj, C. A. Balseiro, D. Feinberg, and M. Avignon, Phys. Rev. Lett. **101**, 107001 (2008).
[21] A. Zazunov, R. Egger, T. Jonckheere, and T. Martin, Phys. Rev. Lett. **103**, 147004 (2009).
[22] T. Yokoyama, M. Eto, and Y. V. Nazarov, Phys. Rev. B **89**, 195407 (2014).
[23] M. A. Silaev, A. Y. Aladyshkin, M. V. Silaeva, and A. S. Aladyshkina, J. Phys.: Condens. Matter **26**, 095702 (2014).
[24] F. Dolcini, M. Houzet, and J. S. Meyer, Phys. Rev. B **92**, 035428 (2015).

[25] C.-Z. Chen, J. J. He, M. N. Ali, G.-H. Lee, K. C. Fong, and K. T. Law, Phys. Rev. B **98**, 075430 (2018).
[26] M. Minutillo, D. Giuliano, P. Lucignano, A. Tagliacozzo, and G. Campagnano, Phys. Rev. B **98**, 144510 (2018).
[27] S. Pal and C. Benjamin, Europhys. Lett. **126**, 57002 (2019).
[28] A. A. Kopasov, A. G. Kutlin, and A. S. Mel'nikov, Phys. Rev. B **103**, 144520 (2021).
[29] P. G. D. Gennes, *Superconductivity of Metals and Alloys* (CRC, Boca Raton, FL, 2018).
[30] M. F. Goffman, C. Urbina, H. Pothier, J. Nygård, C. M. Marcus, and P. Krogstrup, New J. Phys. **19**, 092002 (2017).
[31] J. C. E. Saldaña, R. Žitko, J. P. Cleuziou, E. J. H. Lee, V. Zannier, D. Ercolani, L. Sorba, R. Aguado, and S. D. Fransceschi, Sci. Adv. **5**, eaav1235 (2019).
[32] Z. Scherübl, G. Fülöp, M. H. Madsen, J. Nygård, and S. Csonka, Phys. Rev. B **94**, 035444 (2016).
[33] Ö. Gul, H. Zhang, F. K. D. Vries, J. V. Veen, K. Zuo, V. Muorik, S. Conesa-Boj, M. P. Nowak, D. J. V. Woerkom, M. Quientero-Perez, M. C. Cassidy, A. Geresdi, S. Koelling, D. Car, S. R. Plissard, E. P. A. M. Bakkers, and L. P. Kouwenhoven, ACS Nano Lett. **17**, 2690 (2017).
[34] E. C. Gingrich, B. M. Niedzielski, J. A. Glick, Y. Wang, D. L. Miller, R. Loloee, W. P. Pratt, and N. O. Birge, Nat. Phys. **12**, 564 (2016).
[35] M. Davydova, S. Prembabu, and L. Fu, Sci. Adv. **8**, eabo0309 (2022).
[36] A. Freyn, B. Douçot, D. Feinberg, and R. Mélin, Phys. Rev. Lett. **106**, 257005 (2011).
[37] G. Deutscher, J. Supercond. **15**, 43 (2002).
[38] C. W. J. Beenakker, Phys. Rev. Lett. **67**, 3836 (1991).